Therapeutic effects of bone marrow mesenchymal stem cells on radiation-induced sciatic nerve injury

Y. Zhang*, JP. Zhou, JJ. Zhao, ZC. Zuo, JZ. Qin

Department of Hand and Foot Surgery, The Second Affiliated Hospital of Soochow University, Suzhou, Jiangsu 215004, China

► *Original article*

ABSTRACT

Background: Radiation-induced peripheral neuropathy (RIPN) is one of the severe adverse effects of radiation therapy that significantly reduces patient quality of life. Bone marrow mesenchymal stem cells (BMSCs) exert beneficial effects on nerve regeneration following injury. We hypothesized that BMSCs are a potential treatment option for RIPN. This study aimed to evaluate the radioprotective effects of BMSCs on RIPN in a rat model. **Materials and Methods:** The right sciatic nerves of fifty-four male Sprague-Dawley rats were locally irradiated with a single dose of 30 Gy X-rays. The rats were randomly divided into three groups (n = 18): Radiation control (RC), Radiation + BMSCs (RB) and Radiation + phosphate-buffered solution (RP). BMSCs and phosphate-buffered solution were administered via gastrocnemius muscle injection 24 hours after radiation exposure. Gait analysis, electrophysiological examinations and morphological examinations were performed subsequently. **Results:** No significant differences were observed between the RC and RP groups. Evaluation of the sciatic functional index demonstrated no statistical differences between the three groups after 4, 12 and 24 weeks. The RB group showed better improvement than either RC or RP group, as evidenced by increased motor nerve conductive velocity, expression level of S-100, mean diameter of the axon and thickness of the myelin sheath and decreased perineural scar tissue. **Conclusion:** The present study indicated that BMSCs can improve the electrophysiological and morphological features of radiation exposed sciatic nerves, and have therapeutic potential for RIPN management.

INTRODUCTION

Radiation-induced peripheral neuropathy (RIPN), one of the major adverse effects of radiotherapy, can result in irreversible sensory and motor dysfunction of the extremities [1,2]. The specific pathophysiological mechanism of RIPN development remains unclear; however, the direct effects of radiation on Schwann cells (SCs) and radiation-induced extensive fibrosis in the nerve environment appear to play an important role in the pathogenesis of this neuropathy [3]. After peripheral nerve irradiation, two stages of neuropathy arise and play critical roles in the progression of peripheral neuropathy. The first stage involves electrophysiological, biochemical, and histopathological changes, whereas the second stage involves injury to small arterioles and fibrosis of the soft tissues surrounding the radiation-exposed nerve [4].

Several therapies have been proposed for use after radiation exposure to promote injury healing and tissue regeneration to alleviate RIPN. Currently, supportive and surgical clinical approaches are the primary treatment modalities for RIPN, and neurolysis of the affected nerve from fibrotic tissue is the preferred surgical treatment in clinical practice.

Although neurolysis have shown to relieve pain in clinical studies, sensory or motor function impairments did not appear to recover. Thus, the mere release of the irradiated nerve from fibrosis is insufficient to treat RIPN [5,6]. The role of potentially injured SCs cannot be overlooked for the effective treatment of this type of refractory neuropathy, and dealing with these direct effects on the nerve may be an important aspect of the treatment.

Bone marrow mesenchymal stem cells (BMSCs) repair and replace damaged tissues by differentiating into effector cells, such as SCs and neurons. Thus, BMSCs are a promising treatment option for peripheral nerve injuries. In addition to its anti-inflammatory properties, it protects tissues against radiation-induced injuries by scavenging free radicals [7]. The characteristics of BMSCs make them important therapeutics for radiation-induced injuries. BMSCs have been used in a variety of radiation-induced diseases as an effective post-radiation treatment strategy and play an important role in clinical practice [8-10]. Hence, in view of these properties, we hypothesized that BMSCs could be used as a potential therapy for RIPN. Accordingly, this study aimed to evaluate the radioprotective effects of BMSCs against RIPN in a rat model.

In the present study, we present a novel investigation of the potential protective effects of BMSCs against RIPN. To the best of our knowledge, this is the first study to evaluate the therapeutic role of BMSCs in RIPN using simultaneous functional and histological analyses for a comprehensive analysis of the potential benefits of BMSCs. This approach may provide a new therapeutic strategy for protecting peripheral nerve function during radiation therapy, thereby improving the patients' quality of life.

MATERIALS AND METHODS

Animals

Sixty healthy male Sprague-Dawley (SD) rats weighing 180-200 g were used in this study. Rats were obtained from the Experimental Animal Center of the Medical College of Soochow University, China (SYXK (Su) 2021-0012). This study was approved by the ethical review committee of the Second Affiliated Hospital of Soochow University (approval number: EC2020094). This study was conducted in accordance with the principles of the Declaration of Helsinki. The rats were housed in polycarbonate boxes with rice–husk bedding. They were housed under the following conditions: a temperature of 21°C, relative humidity of 50-70%, air flow rate of 15 exchanges per hour and a light/dark cycle of 12/12 h with free access to food and fresh tap water.

Isolation and culture of BMSCs

Six SD rats were euthanized using an overdose of pentobarbital sodium. The bilateral tibias and femurs of the rats were immediately harvested under sterile conditions. To expose the bone marrow cavity, the epiphyses on each side of the femur and tibia were cut and rinsed with phosphate buffered solution (PBS, Gibco, USA). The bone marrow filtrate was collected and centrifuged at 800 rpm for 5 min. The supernatant was discarded, and the cells were resuspended in low-glucose Dulbecco's Modified Eagle's medium (L-DMEM, Gibco) and placed in a 10 mL culture dish containing 10% fetal bovine serum (FBS, Gibco) and 1% penicillin/streptomycin. The BMSCs were cultured at 95% humidity with 5% CO_2 at 37°C. Half the culture medium volume was changed after 48 h, and the medium was replaced every three days. The cells were passaged when the cell confluence reached approximately 80%. BMSCs at passage 3 were used for subsequent experiments.

Detection of surface antigen molecular expression

The expression of cell surface markers on BMSCs was analyzed using flow cytometry. Passage 3 BMSCs were rinsed twice with PBS, trypsinized with 0.25% trypsin (Sigma, USA) into cell suspension, centrifuged for 5 min at 800 rpm, and adjusted to a cell density of approximately $1×10^6$ cells/mL. Thereafter, 100 µL of the cell suspension was incubated with phycoerythrin (PE) or fluorescein isothiocyanate (FITC)-labeled mouse anti-rat CD29 (1:200), CD34 (1:200), CD45 (1:100) and CD90 (1:200) monoclonal antibodies (eBioscience, USA) at 37°C in the dark for 30 min and tested using a FACS Calibur flow cytometry apparatus coupled with Cell Quest Pro Software (Beckman Coulter, USA).

Radiation procedure

Rats were anesthetized using an intraperitoneal injection of pentobarbital sodium (40 mg/kg) before radiation. Their right legs were exposed to a single local dose of 30 Gy from an X-ray teletherapy device at a rate of 200 cGy/min via the 6 MV photon beam of a medical electron linear accelerator (Primus, Siemens Medical Systems, USA). The length × width of the field was 40 × 40 mm, which was centered around the posterior thigh and buttock with a silicone gel bolus (0.5 cm) to ensure 100% dose to the skin. Other body parts of the rats were protected by lead and beam collimation.

Groups and transplantation procedure

Twenty-four hours after irradiation, the BMSCs used for qualitative (immunohistochemical) assays were tagged with 5-bromo-2-deoxyuridine (BrdU; Abcam, UK) 48 h prior to transplantation. Approximately $1×10^6$ BMSCs were prepared in 1 mL total fluid volume of PBS for this study. Fifty-four rats were randomly divided into three groups (n = 18): radiation control (RC), no treatment administered after radiation, radiation + BMSCs (RB), 1 mL PBS with BMSC suspensions injected into the medial and lateral heads of the gastrocnemius muscle after radiation, radiation + PBS (RP), 1 mL PBS injected into the medial and lateral heads of the gastrocnemius muscle after radiation.

The animals were euthanized 24 weeks after irradiation for electrophysiological examination, hematoxylin and eosin (HE) staining, immunohistochemical staining for S-100, BrdU and ultrastructural observation. All measurements were performed by an investigator who was blinded to the experimental allocation.

Walking track analysis of sciatic functional index

Walking track analysis was performed at 4, 12 and 24 weeks after irradiation. Six rats were randomly selected from each group and evaluated on a confined walking track that was 8.2 cm width and 42 cm long, with a dark shelter at the end. A piece of paper was placed on the floor of a walking corridor. Black ink was applied to the plantar surfaces of both hind limbs of each rat. The rats were permitted to walk to the shelter, leaving black footprints on the paper. This was repeated three times in one session, and the footprints were scored using the sciatic functional index (SFI). The lengths of the third toe to the heel (PL), of first to fifth toe (TS) and of second to fourth toe (ITS) on the experimental side (EPL, ETS and EIT,

respectively) and the contralateral (normal) side (NPL, NTS, and NIT, respectively) were measured in each rat. The SFI for each rat was calculated using following formula: SFI = −38.3 × (EPL − NPL)/NPL + 109.5 × (ETS − NTS)/NTS + 13.3 × (EITS − NITS)/NITS − 8.8. The SFI score generally oscillates around 0, indicating normal nerve function; a score of approximately −100 indicates complete loss of function.

Electrophysiological assessment

Electrophysiological analysis was performed twenty-four weeks after radiation. Six rats from each group were randomly selected and anesthetized. The irradiated sciatic nerves were exposed, stimulation electrodes were placed on the sciatic nerve trunk, a recording electrode was placed on the gastrocnemius muscle and a ground electrode was placed on the subcutaneous tissue. Electrical stimulation ranging from 1 to 20 mA was applied, with a frequency of 1 Hz and duration of 0.1-0.2 ms. The latency of onset and peak amplitude of the compound muscle action potential (CMAP) were recorded using a multimedia electromyogram (M314636, NHK30, Medelec Synergy, UK) and the motor nerve conductive velocity (MNCV) value was calculated.

Evaluation of perineural scar tissue

After electrophysiological evaluation twenty-four weeks later, six rats from each group were randomly selected for gross morphological observations of the irradiated site. The fibrous connective tissue surrounding the irradiated site was examined under a surgical microscope. Scar severity and nerve adherence were evaluated using Petersen's numerical grading scheme for macroscopic assessment [11].

Tissue harvest

The perineural scar tissue was evaluated, and the rats were euthanized using an overdose of anesthesia 24 weeks after radiation. Irradiated sciatic nerve specimens were dissected from the right leg approximately 1 cm proximal to the trifurcation, for HE staining, immunohistochemical analysis, and ultrastructural observation.

Histological observation

Six irradiated nerve specimens were harvested from each group and fixed in 10% formaldehyde. After fixation, specimens were embedded in paraffin blocks. All specimens were cut into transverse slices and stained with HE (Sinopharm, Beijing, China). The structures and cell proliferation were then observed under a light microscope (BX51T-PHD-J11, Olympus, Japan) and photographed using a digital camera (EOS550D, Canon, Japan) attached to the microscope.

Immunohistochemical analysis

Six irradiated nerve specimens from each group were washed with PBS and preserved in a 10% formaldehyde solution at 4°C overnight. Specimens were dehydrated using an escalating alcohol series, beginning with 70% ethanol, and then embedded in paraffin blocks. Transverse slices (5 μm thick) were placed on Poly-L-lysine-coated slides overnight at 60° C. The slides were successively incubated overnight with primary antibodies of rabbit monoclonal anti-S-100 (1:200, Sigma) and mouse monoclonal anti-BrdU (1:200, Sigma) at 4°C, rinsed with PBS and incubated with the appropriate secondary antibodies of biotin-conjugated goat anti-mouse IgG (1:100, Sigma) at room temperature for 1 h. After rinsing with PBS, the slides were incubated with horseradish peroxidase-conjugated streptavidin (1:100, Sigma) for 1 h. Sections were then incubated with hematoxylin (Sinopharm, Shanghai, China) for nuclear counterstaining. All sections were examined in five randomly selected fields at 40× magnification using a light microscope (BX51T-PHD-J11; Olympus, Japan) and photographed using a digital camera (EOS550D, Canon, Japan) attached to the microscope. Digital images were analyzed using a computer-based morphometry software (WinROOF, Mitani, Japan). The areas of positive nuclear and cytoplasmic stained cells (%) for S-100 and BrdU immunohistochemistry were determined using automatically computed parameters.

Ultrastructural observation

Six irradiated nerve specimens from each group were preserved in cold-buffered 4% glutaraldehyde solution (Sigma). The nerves were then immersed in a 1% osmium tetroxide solution (Sanger, China) for 1 h, dehydrated with an escalating acetone series beginning with 30% acetone and embedded in Araldite 502 (Polysciences, USA) for 2 h. A Leica EM UC6 Ultramicrotome (Leica, Germany) was used to obtain ultrathin slices of 60 nm thickness. The tissue sections were stained with 1% uranyl acetate and lead citrate (Baoman, Shanghai, China). Nerve sections were observed under a transmission electron microscope (TEM, H-600, Hitachi, Japan) and photographed using a digital camera (EOS550D, Canon, Japan) attached to the microscope at 4000× and 10000 × magnification.

Statistical analysis

Statistical analyses were performed using SPSS 21.0 statistics software (SPSS, USA). Data were analyzed by one-way analysis of variance and Tukey's post hoc test and expressed as the mean ± standard error of the mean. *p*-values < 0.05 were considered statistically significant.

RESULTS

Characterization of cultured BMSCs

By 24 h after initial plating, the adhering cells

developed a tiny rounded, spindle-shaped morphology (figure 1A). By day 7, the attached BMSCs had developed into an adherent layer with several distributed spindle-like cells (figure 1B). By day 14, the primary BMSCs formed a nearly continuous layer composed mainly of spindle-like cells (figure 1C). At passage 3, the fibroblast-like cells were morphologically homogenous with > 80% purity (figure 1D). Flow cytometric analysis showed that the cells were immunopositive for CD90 (98.9%, figure 1E), CD29 (93.7%, figure 1F), CD45 (1.3%, figure 1G) and CD34 (0.8%, figure 1H).
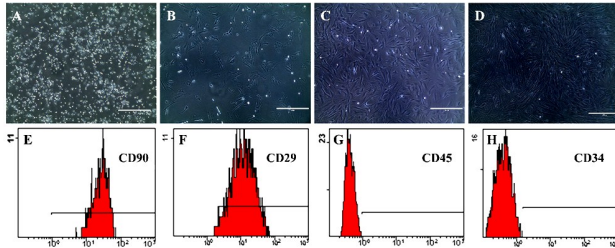
Figure 1. Phase-contrast microscopic images revealing the morphological characteristics of cultured BMSCs at 24 h **(A)**, day 7 **(B)** and day 14 **(C)** and passage 3 **(D)**. Scale bar = 400 μm. Phenotypes of cultured BMSCs as observed by flow cytometry. **(E)** CD90, **(F)** CD29, **(G)** CD45 and **(H)** CD34.

Functional assessment

The evaluation of SFI demonstrated no statistically significant differences among the three groups at 4, 12 and 24 weeks after radiation ($P > 0.05$, figure 2).
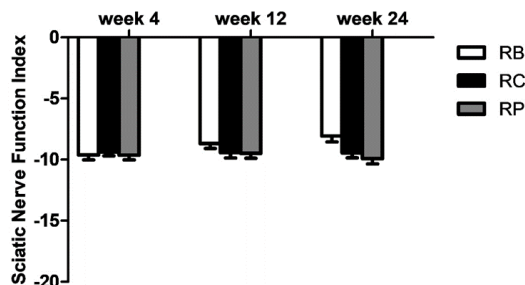

Figure 2. Walking track recovery as evaluated by the SFI value of the three groups at weeks 4, 8 and 12 after radiation.

Electrophysiological examination

The RB group had significantly shorter latencies for CMAP onset than those of the RC or RP groups ($P < 0.05$) and there were no statistically significant differences between the RC and RP groups ($P > 0.05$). The RB group had significantly higher peak amplitudes of CMAP and MNCV than those of the RC and RP groups ($P < 0.05$) and the RC and RP groups did not differ significantly ($P > 0.05$, figure 3). Thus, BMSCs significantly reduced the latency of onset, elevated the peak amplitude of CMAP, and improved sciatic nerve motor conduction velocity compared to those in untreated and PBS-treated animals.

Evaluation of perineural scar tissue

The irradiated nerves were surrounded and tethered by thick, tenacious epineurial scar tissue in the RC and RP groups. Nerve isolation and separation often requires strong, blunt, or violent dissection. A small lucent membrane enveloped the irradiated nerves in the RB group. There was less scarring, and the nerve was less tenacious and easily separated from the surrounding tissue in the RB group compared to those in the RC or RP groups. The RB group had significantly lower nerve adhesion and nerve separability scores than those of the RC and RP groups ($P<0.05$). There were no significant differences between the RC and RP groups ($P > 0.05$, figure 4). The untreated and PBS-treated animals showed scar-like formations around the exposed nerves, whereas treatment with BMSCs inhibited these effects.
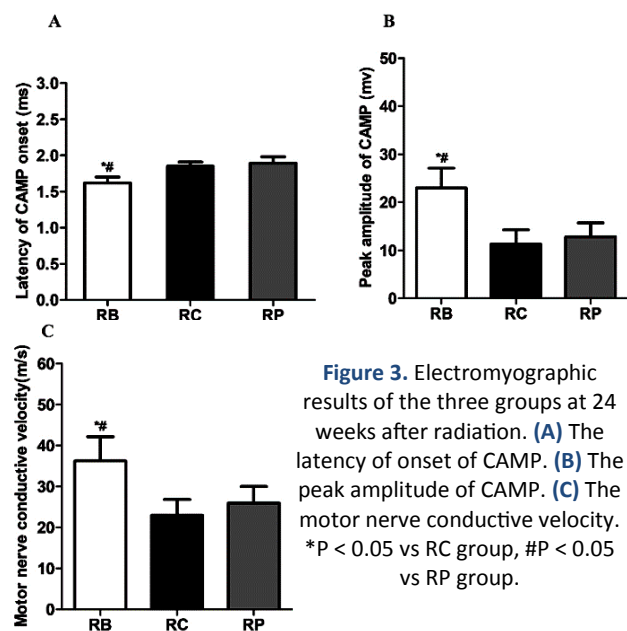

Figure 3. Electromyographic results of the three groups at 24 weeks after radiation. **(A)** The latency of onset of CAMP. **(B)** The peak amplitude of CAMP. **(C)** The motor nerve conductive velocity. *P < 0.05 vs RC group, #P < 0.05 vs RP group.

Figure 4. Comparison of the scores for nerve adherence and nerve separability among the three groups at the end of 24 weeks after radiation. *P < 0.05 vs RC group, #P < 0.05 vs RP group.
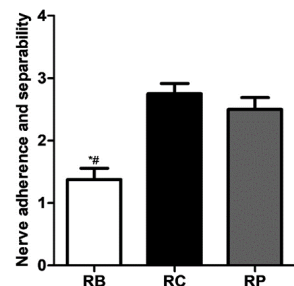
Histological examination

HE staining revealed that the tissue structure was slightly loosened in the RB group. The irradiated nerve fibers were densely dispersed, with a few inflammatory cells scattered around the axons. The tissue structure was loosened in both the RC and RP groups. The nerve fibers were sparsely dispersed, and numerous inflammatory cells infiltrated the axons (figure 5A). The results showed that the BMSC-treated group displayed fewer inflammatory infiltrates and endoneurial collagen in the nerves than that displayed by the non-treated or PBS-treated animals.
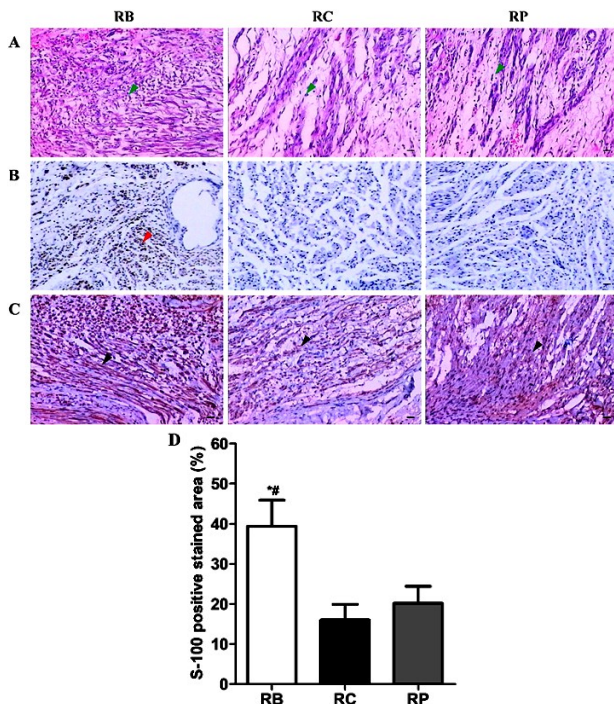
Figure 5. (A) HE staining results of the irradiated nerves at the end of 24 weeks after radiation. The green arrows indicate inflammatory cells. Immunohistochemical staining results of BrdU **(B)** and S-100 **(C)** of the irradiated nerves at the end of 24 weeks after radiation. The red arrow indicates BrdU-immunopositive cells. The black arrows indicate S-100-immunopositive cells; Scale bar = 100 μm. **(D)** Quantitative analysis of immunostaining for S-100 among groups. *P < 0.05 vs RC group, #P < 0.05 vs RP group.

Immunohistochemical analysis

Immunohistochemical detection of the irradiated nerves showed many BrdU-positive cells in the RB group but not in the RC or RP groups (figure 5B). Immunohistochemical staining revealed varying degrees of S-100-positive cells with brown-stained nuclei in the three groups (figure 5C). The RB group showed higher levels of S-100 expression than did the RC or RP groups ($P < 0.05$), whereas there were no significant differences between the RC and RP groups ($P > 0.05$ and figure. 5D). The results showed that BMSCs could migrate to radiation-damaged sites, and the BMSC treatment group was more effective than the non-treated or PBS-treated groups in promoting SC migration and proliferation.

Ultrastructural observation

TEM revealed that the irradiated myelin sheaths in the RB group were round or oval. These layers showed slight axonal swelling, myelin sheath vacuolization and distortion. In both RC and RP groups, the axons experienced significant swelling, myelin sheath vacuolization and distortion. The layers were distinct and the structure was obscured by vacuole degeneration (figure 6A and B). The RB group showed a considerably higher average myelin sheath thickness and axon diameter than those of the RC or RP groups ($P < 0.05$). No statistically significant

differences were observed between the RC and RP groups ($P > 0.05$, figure 6C and D). The results indicated varying degrees of axonal degeneration and demyelination induced by radiation. The axonal structure in the BMSC-treated group was almost normal. The diameter and thickness of the myelin sheaths in the BMSC-treated group were significantly greater than those in the untreated or PBS-treated groups.
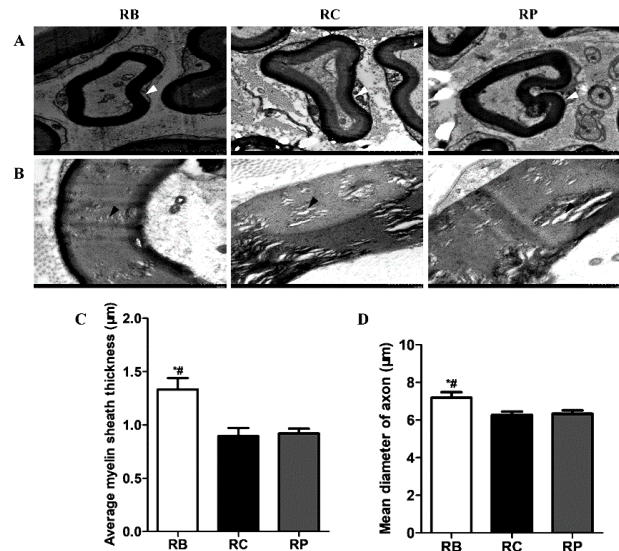

Figure 6. TEM images showing the morphology of axons and myelin sheaths at the end of 24 weeks after radiation. **(A)** White arrows show distortion of the axons. Scale bar = 2 μm. **(B)** Black arrows show vacuole degeneration. Scale bar = 500 nm. **(C)** Comparison of the average of myelin sheath thickness among groups. **(D)** Comparison of the mean axon diameter among groups. *P < 0.05 vs RC group, #P < 0.05 vs RP group.

DISCUSSION

RIPN is a well-known complication of radiation therapy. Radiation-induced nerve damage is thought to be caused by an initial microvascular injury that leads to delayed nerve injury via radiation-induced fibrosis, eventually leading to RIPN. Symptoms can progress and usually appear years after the initial treatment, with the nerve injury site being consistent with the location of radiation delivery. RIPN is thought to possess a threefold pathogenesis. The first phase involves chronic local inflammation, which leads to the second stage during which fibroblasts and myofibroblasts are overactivated, resulting in considerable active fibrosis by transforming growth factor beta 1 protein. The third phase, the late fibrotic-atrophic phase, results in loss of parenchymal cells and reduced capillary vascularity [12]. This process leads to direct axonal injury and demyelination, extensive fibrosis within and surrounding nerve trunks, and ischemia of the arteries supplying the nerves [13].

Radiation-induced injury can be prevented using chemical compounds, biological agents, Chinese

herbal extracts or cellular therapies [14,15]. These measures can reduce or improve radiation-induced tissue damage and promote recovery. BMSCs protect normal tissues from radiotherapy complications [8-10,16]. Because they can scavenge free radicals with low toxicity and few adverse effects [7,17], they are an effective treatment strategy for several radiation-induced disorders. BMSCs can not only differentiate into SCs but also transform into SCs directly at the site of injury and promote nerve regeneration by releasing neurotrophic and growth factors, as well as myelin basic protein [18,19]. The administration of BMSCs can regulate the activity of native SCs, modify the inhibitory regenerative environment, improve myelination and cell survival, and enhance neurotrophic activity. BMSCs secrete a variety of cytokines, such as interleukin-6 and granulocyte colony-stimulating factor, compensating for radiation-induced deficiencies in cytokines to inhibit neuroinflammation [20].

Our results showed no significant differences among the three groups in terms of SFI after 4, 12 and 24 weeks. This finding aligns with the findings from previous studies that demonstrated that radiation led to no change in motor nerve function. Lin *et al.* reported that motor function assessments in rabbit sciatic nerves treated with a single dose of 25 Gy radiation remained intact after three, five, and seven months. Insufficient follow-up time may be one of the reasons for the lack of changes in motor nerve function [21]. Clinical observations have demonstrated that symptoms of neuropathy might occur 6 months or a few years after radiation, the average interval was calculated as 1-4 years [22].

The inflammatory response at the site of exposure plays a significant role in the development of radiation-induced diseases. The inflammatory cytokines and chemokines expressed abundantly in injured tissues recruit inflammatory cells from the peripheral blood to migrate to the injured site. Inflammatory cells produce oxidatively active chemicals that cause additional damage to tissue cells [23]. In our study, we found a large number of inflammatory cells infiltrating the irradiated sciatic nerves of rats in the non-treated and PBS-treated control groups 24 weeks after radiation. In contrast, the number of inflammatory cells was decreased in the sciatic nerves of rats treated with BMSCs. This finding agrees with previous studies demonstrating that BMSCs can ameliorate radiation-induced chronic and acute inflammation [24,25]. At 24 weeks, the RC and RP groups exhibited scar-like formations around the exposed nerves, whereas treatment with BMSCs inhibited these effects. Our findings are consistent with those of the study by Okuda *et al.* [26], which showed that BMSCs might promote axonal regeneration and functional recovery while suppressing scar formation. Studies by Aktas *et al.* [27] and Okuhara *et al.* [6] demonstrated histopathological

changes in terms of axonal degeneration and demyelination of the sciatic nerve after high-dose radiation. The histological results from our study were consistent with the conclusions of these studies. Furthermore, in the present study, the histological results of the RC and RP groups showed significant nerve damage; however, BMSCs ameliorated this effect. The findings of this study indicate that BMSCs can prevent RIPN via anti-inflammatory and multidirectional differentiation effects and their ability to regulate physiological and pathological processes.

CONCLUSION

In the present study, BMSCs inhibited the local inflammatory response, promoted the movement of BMSCs to radiation-injured nerve tissues, and showed the potential to improve electrophysiological and morphological features of irradiated sciatic nerves. Hence, BMSCs could be a potential tool against radiotherapy-induced peripheral neuropathy and with therapeutic effects in RIPN management.

REFERENCES

1. Delanian S, Lefaix JL, Pradat PF (2012) Radiation-induced neuropathy in cancer survivors. *Radiother Oncol*, **105:** 273-282.
2. Zhu Y, Tsai W, Sokolof J (2021) Sciatic neuropathy after radiation treatment. *Am J Phys Med Rehabil*, **100:** e198-e199.
3. Gikas PD, Hanna SA, Aston W, Kalson NS, Tirabosco R, Saifuddin A, Cannon SR (2018) Post-radiation sciatic neuropathy: a case report and review of the literature. *World J Surg Oncol,* **6:** 130.
4. Shabeeb D, Musa AE, Keshavarz M, Esmaely F, Hassanzadeh G, Shirazi A, Najafi M (2019) Histopathological and Functional Evaluation of Radiation-Induced Sciatic Nerve Damage: Melatonin as Radioprotector. *Medicina(Kaunas),* **55:** 502.
5. Gillette EL, Mahler PA, Powers BE, Gillette SM, Vujaskovic Z (1995) Late radiation injury to muscle and peripheral nerves. *Int J Radiat*

Oncol Biol Phys, **31**: 1309-1318.

6. Okuhara Y, Shinomiya R, Peng F, Kamei N, Kurashige T, Yokota K, Ochi M (2014) Direct effect of radiation on the peripheral nerve in a rat model. *J Plast Surg Hand Surg*, **48**: 276-280.

7. Stavely R, Nurgali K (2020) The emerging antioxidant paradigm of mesenchymal stem cell therapy. *Stem Cells Transl Med*, **9**: 985-1006.

8. Lim JY, Yi T, Choi JS, Jang YH, Lee S, Kim HJ, Song SU, Kim YM (2013) Intraglandular transplantation of bone marrow-derived clonal mesenchymal stem cells for amelioration of post-irradiation salivary gland damage. *Oral Oncol*, **49**: 136-143.

9. Zheng K, Wu W, Yang S, Huang L, Chen J, Gong C, Fu Z, Lin R, Tan J (2016) Treatment of radiation-induced acute intestinal injury with bone marrow-derived mesenchymal stem cells. *Exp Ther Med*, **116**: 2425-2431.

10. Xia C, Chang P, Zhang Y, Shi W, Liu B, Ding L, Liu M, Gao L, Dong L (2016) Therapeutic effects of bone marrow-derived mesenchymal stem cells on radiation-induced lung injury. *Oncol Rep*, **35**: 731-738.

11. Petersen J, Russell L, Andrus K, MacKinnon M, Silver J, Kliot M (1996) Reduction of extraneural scarring by ADCON-T/N after surgical intervention. *Neurosurgery*, **38**: 976-983. discussion 983-984.

12. Manne R, Thakkar P, Zheng J (2021) Radiation-Induced Obturator Nerve Injury in Cervical Cancer. *J Rehabil Med Clin Commun*, **4**: 1000043.

13. Delanian S, Lefaix JL, Pradat PF (2012) Radiation-induced neuropathy in cancer survivors. *Radiother Oncol*, **105**: 273-282.

14. Patyar RR, Patyar S (2018) Role of drugs in the prevention and amelioration of radiation induced toxic effects. *Eur J Pharmacol*, **819**: 207-216.

15. Mun GI, Kim S, Choi E, Kim CS, Lee YS (2018) Pharmacology of natural radioprotectors. *Arch Pharm Res*, **41**: 1033-1050.

16. Chapel A (2012) Stem Cells and Irradiation. *Cells*, **10**: 760.

17. Chen MF, Lin CT, Chen WC, Yang CT, Chen CC, Liao SK, Liu JM, Lu CH, Lee KD (2006) The sensitivity of human mesenchymal stem cells to ionizing radiation. *Int J Radiat Oncol Biol Phys*, **66**: 244-253.

18. Wang J, Ding F, Gu Y, Liu J, Gu X (2009) Bone marrow mesenchymal stem cells promote cell proliferation and neurotrophic function of Schwann cells *in vitro* and *in vivo*. *Brain Res*, **1262**: 7-15.

19. Sayad Fathi S and Zaminy A (2017) Stem cell therapy for nerve injury. *World J Stem Cells*, **9**: 144-151.

20. Qiao S, Ren H, Shi Y, Liu W (2014) Allogeneic compact bone-derived mesenchymal stem cell transplantation increases survival of mice exposed to lethal total body irradiation: a potential immunological mechanism. *Chin Med J (Engl)*, **127**: 475-482.

21. Lin Z, Wu VW, Ju W, Yamada Y, Chen L (2011) Radiation-induced changes in peripheral nerve by stereotactic radiosurgery: a study on the sciatic nerve of rabbit. *J Neurooncol*, **102**: 179-185.

22. Stoll BA, Andrews JT (1966) Radiation-induced Peripheral Neuropathy. *Br Med J*, **1**: 834-837.

23. Zhao W, Robbins ME (2009) Inflammation and chronic oxidative stress in radiation-induced late normal tissue injury, therapeutic implications. *Curr Med Chem*, **16**: 130-143.

24. Horton JA, Hudak KE, Chung EJ, White AO, Scroggins BT, Burkeen JF, Citrin DE (2013) Mesenchymal stem cells inhibit cutaneous radiation-induced fibrosis by suppressing chronic inflammation. *Stem Cells*, **31**: 2231-2341.

25. Hou G, Li J, Liu W, Wei J, Xin Y, Jiang X (2022) Mesenchymal stem cells in radiation-induced lung injury: From mechanisms to therapeutic potential. *Front Cell Dev Biol*, **10**: 1100305.

26. Aktas S, Comelekoglu U, Yilmaz SN, Yalin S, Arslantas S, Yilmaz BC, Sogut F, Berkoz M, Sungur MA (2013) Electrophysiological, biochemical and ultrastructural effects of radiotherapy on normal rat sciatic nerve. *Int J Radiat Biol*, **89**: 155-161.

27. Okuda A, Horii-Hayashi N, Sasagawa T, Shimizu T, Shigematsu H, Iwata E, Morimoto Y, Masuda K, Koizumi M, Akahane M, Nishi M, Tanaka Y (2017) Bone marrow stromal cell sheets may promote axonal regeneration and functional recovery with suppression of glial scar formation after spinal cord transection injury in rats. *J Neurosurg Spine*, **26**: 388-395.